Journal of Materials Chemistry C

Accepted Manuscript

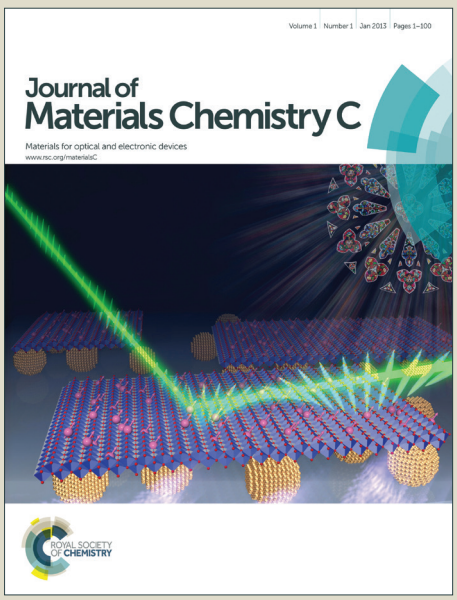

ROYAL SOCIETY OF CHEMISTRY

www.rsc.org/materialsC

Journal of Materials Chemistry C RSCPublishing

PAPER

Enhanced Dielectric Properties of PVDF-HFP/$BaTiO_3$-nanowires Composites Induced by Interfacial Polarization and Wire-shape

Cite this: DOI: 10.1039/x0xx00000x

Received 00th January 2012,
Accepted 00th January 2012

DOI: 10.1039/x0xx00000x

www.rsc.org/

Y Feng,[a] W. L. Li, [*a, b] Y. F. Hou,[a] Y Yu,[a] W. P. Cao,[a] T. D. Zhang,[a] and W.D. Fei,[a, c]

Polymer based composites with high dielectric constant were successfully fabricated by using $BaTiO_3$ nanowires with high aspect ratio as inorganic filler and PVDF-HFP as polymer matrix. PVDF-HFP/$BaTiO_3$ nanoparticles composites were also prepared as a contrast. The $BaTiO_3$ nanowires were synthesized via one-step hydrothermal method. The $BaTiO_3$ nanowires and two types of composites were characterized by X-ray diffraction, fourier transform infrared spectroscopy, scanning electron microscope and transmission electron microscopy. For composites, breakdown strength measurements, tensile tests and broadband dielectric spectroscopy analyses were also carried out. The results show that two kinds of fillers are dispersed homogeneously in the matrix. The dielectric constant of composites filled by $BaTiO_3$ nanowires is larger than that filled by $BaTiO_3$ nanoparticles at same content. Stronger interfacial polarization was found in PVDF-HFP/$BaTiO_3$ nanowires composites. Two theoretical models were employed to predict the dielectric constants of composites, and the experimental data were consistent with the estimated trend. The enhanced dielectric properties of PVDF-HFP/$BaTiO_3$ nanowires composite are attributed to the superior interfacial polarization and high aspect ratio of $BaTiO_3$ nanowires.

Introduction

Dielectric materials with high dielectric constant have a variety of applications in capacitors, gate dielectrics actuators and electric stress control.[1-7] Because of the ease of processability and low cost, polymer-based materials with high dielectric constant become more and more important for dielectric applications. Most of pure polymers for dielectric applications have low dielectric constant (e.g, <10). Therefore, current studies have mainly focused on the fabrication of high dielectric constant and low dielectric loss polymer composites and the interfacial improvement between organic-inorganic.[8-12] So far several methods have been developed to prepare polymer composites with high dielectric constant. One classic approach is to introduce high dielectric constant ceramic nanoparticles (e.g., $BaTiO_3$) into a polymer.[13-16]

Recently, many efforts have been devoted to the development of high-ε composites based on PVDF and its derivative copolymers.[17-20] Poly(vinylidene fluoride) (PVDF), which is a semicrystalline thermoplastic polymer with remarkable high piezo- and pyroelectric coefficient, excellent thermal stability and chemical resistance, and its derivative copolymers such as poly(vinylidene fluoride-co-trifluoroethylene [P(VDF-TrFE)], poly(vinylidene fluoride-co-hexafluoropropylene) [PVDF-HFP] and poly(vinylidene fluoride-trifluoroethylene-chlorofluoroethylene) [P(VDF-TrFE-CFE)] have been employed to fabricate high-ε composites. However, the largest disadvantage of ceramic/polymer based composites is that the high volume fraction (>50 vol%) of the filler is necessary to fabricate high-ε composites. So many inorganics in the polymer matrix must cause high mass density, low flexibility, and poor mechanical performance of the composites.[2, 13] To overcome these limitations of the composite, promising work has recently been conducted based on high aspect ratio ceramic fillers.[21, 22] Firstly, many models have shown that high aspect ratio fillers can improve the dielectric constant of the composites.[23] Several researchers have also demonstrated that filler with high aspect ratio can improve the dielectric constant of the composites more efficiently as compared to spherical particles because percolation threshold of filler with high aspect ratio is lower than that of particles.[24-26] The percolation threshold is strongly dependent on the filler morphology. Theoretically, the high aspect ratio fillers reach the percolation threshold easier than the low aspect ratio fillers, which allows

[a] *School of Materials Science and Engineering, Harbin Institute of Technology, Harbin 150001, P.R. China*

[b] *National Key Laboratory of Science and Technology on Precision Heat Processing of Metals, Harbin Institute of Technology, Harbin 150001, P.R. China. Email: wlli@hit.edu.cn*

[c] *State Key Laboratory of Advanced Welding and Joining, School of Materials Science and Engineering, Harbin Institute of Technology, Harbin 150001, P.R. China.*

connectivity or continuous passage in the system and improves the dielectric properties of the composites. In addition, Brunauer−Emmer−Teller (BET) surface area analysis has demonstrated that the high aspect ratio fillers have lower surface area than low aspect ratio fillers, which helps reduce the surface energy, thus preventing agglomeration and enhancing overall performance in the composites. H. X. Tang et al. have fabricated some kinds of nanocomposites with high dielectric constant and low dielectric loss consisting of one dimensional perovskite nanowires and polymer matrix, in the end enhanced the dielectric properties and energy storage density of composites;[27-30] N. Guo et al. have reported on the preparation of polymer/ellipsoid-shaped TiO_2 composites with high dielectric constant;[31] Y. Song et al. fabricated $BaTiO_3$ nanofibers via electrospinning and epoxy/$BaTiO_3$ nanofibers composites.[32] He found that composites filled by $BaTiO_3$ nanofibers exhibited greater dielectric constant and higher breakdown strength than the composites filled by $BaTiO_3$ nanoparticles. These fundamental discoveries have led many researches to follow this route to prepare composites with enhanced dielectric constant. However, the composites filled by high aspect ratio fillers still have not been investigated as extensively as spherical fillers because of challenges in manufacturing nanowires. A majority of works have been reported about the influence of nanowires on the dielectric constant, ferroelectric properties and energy storage density of polymer based composites. No study involving comprehensive analysis (dielectric constant, dielectric loss, electrical breakdown strength, AC conductivity, dielectric modulus formalism et al.) of the composites filled by lower content (≤10 vol%) nanowires has been reported.

Herein, we report a combined approach for enhancing the dielectric properties of composites. Poly(vinylidene fluoride-trifluoroethylene) (PVDF-HFP) is employed as the polymer matrix. Instead of spherical $BaTiO_3$ nanoparticles, $BaTiO_3$ nanowires fabricated via one-step hydrothermal method are used as dielectric fillers. The purpose in our study is to obtain high-ε composites with lower ceramic content (≤10 vol%). In the present study, $BaTiO_3$ nanowires can give rise to increased dielectric constant of the composites with lower ceramic content (≤10 vol%). The influence of nanowires on the dielectric properties under the broadband (10^{-2}-10^{7} Hz) is researched. Finally, the analysis focusing on enhanced dielectric constant in the PVDF-HFP/$BaTiO_3$ nanowires composites is also given. The fabrication process of $BaTiO_3$ nanowires is simple and timesaving in this study. Therefore, the results and methods presented here can be widely applied to the manufacture of high-ε capacitors in the future.

Experimental

Materials

PVDF-HFP pellet was purchased from Sigma-Aldrich Co. Ltd. $BaTiO_3$ nanoparticles, or BT-NPs for short purchased from Aladdin Industrial Corporation with the size of 100nm were sieved out prior to use. $BaTiO_3$ nanowires, or BT-NWs for short were fabricated via hydrothermal method, and the preparation process was shown in the next section. Potassium hydroxide (KOH), polyethylene glycol (PEG 6000), tetrabutyl titanate (TBOT), Barium hydroxide octahydrate ($Ba(OH)_2$ $8H_2O$), formic acetic acid, and ethanol were purchased from Shanghai Chemical Corp. All chemicals were used without further purification. All other chemicals were obtained as analytical grade products and used without further purification.

Preparation of BT-NWs and PVDF-HFP composites

1.5 g PEG6000 was dissolved into ethanol. A solution of 15 mL ethanol containing 1.5 mmol TBOT was then added with fast stirring. After that, KOH alkaline solution was added. The mixture was stirred vigorously for 60 min and then transferred into a Teflon-lined stainless-steel autoclave. Then, 0.473 g $Ba(OH)_2$ $8H_2O$ was added. The autoclave was heated at 200 ℃ for 12 h, which was subsequently cooled to room temperature. The products were centrifuged and rinsed with formic acid, ethanol, and deionized water several times, and dried in vacuum.[33]

The PVDF-HFP/$BaTiO_3$ composites were prepared via an in-situ dispersive polymerization. The BT-NPs or BT-NWs were ultrasonically dispersed in N,N-Dimethylformamide (DMF) for 0.5 h. Then PVDF-HFP pellet was added into the system with mechanical stir for 2 h at 70 ℃. Then the mixture was cast on clean glass plates and dried at 120 ℃ for 2 h in an oven. The prepared composites were filled with various filler concentration and thickness of composites is about 25-35 μm.

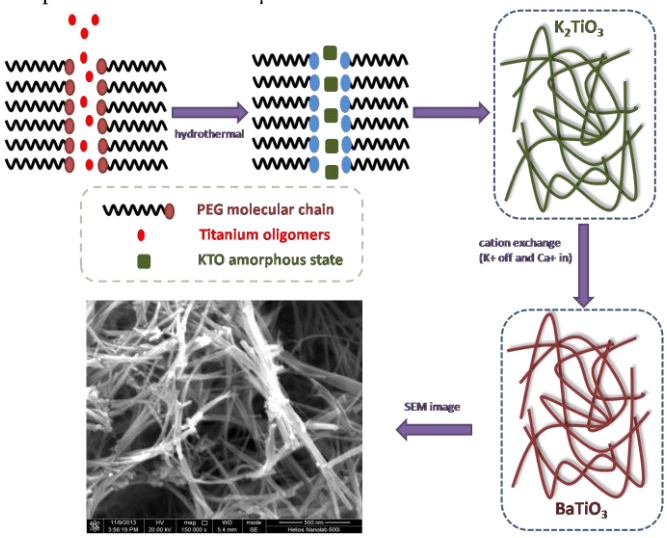

Scheme 1. Schematic diagram of the preparation of $BaTiO_3$ nanowires

Characterization

Fourier transform infrared (FTIR) spectra were measured employing a Nicolet 380 spectrometer by incorporating the sample in a KBr disk.

The scanning electron microscope (SEM) observation was performed on a Helios Nanolab 600i. All samples were prepared by fracturing the composites at liquid nitrogen temperature and then sputter-coated with a homogeneous gold layer to avoid accumulation of charges.

Transmission electron microscopy (TEM) image of synthesized $BaTiO_3$ nanowires was obtained from a JEOL JEM-2100 instrument operated at an accelerating voltage at 200 kV.

The wide-angle X-ray diffraction (XRD) experiments were

performed on an X'pert diffractometer using a CuKα source with an emission current of 40 mA and a voltage of 40 kV.

The broadband dielectric spectroscopy were carried out using a Novocontrol Dielectric Spectrometer (GmbH Germany), CONCEPT 40. The complex permittivity $\varepsilon(\omega) = \varepsilon'(\omega) - i\varepsilon''(\omega)$ has been determined in the frequency (ω) range from 10^{-2} to 1×10^{7} Hz. Prior to dielectric measurements, gold electrodes were deposited onto both surfaces of the specimens by sputtering. The relative humidity (≈50%) of the measurement environment remained constant throughout the investigation and temperature varied in the range of 30-112 ℃.

The breakdown strength measurement was performed according to standard of IEC 243. The samples were placed between two standard electrodes in the silicon oil and with voltage increased at a rate of 1 kV/s until breakdown occured. Five measurements were taken for each specimen group, the average values of electrical breakdown strengths were calculated and used in subsequent analysis.

Tensile tests were performed on a tensile test machine (Instru-Met Corp.). Tensile test samples obtained from the above composite fabrication steps had a nominal gauge length of 20 mm, a width of 10 mm, and a thickness of 25 μm. The samples were loaded in constant deformation mode at a speed of 3 mm/min. Three samples were used for each test.

Results

Characterization of BT-NWs

XRD pattern of the as-synthesized BT-NWs is given in Fig. 1(a). All the diffraction peaks can be assigned to the tetragonal phase of BT without any impurity, in good agreement with the reported data (JCPDS, 81-2203). Representative SEM image of BT-NWs is shown in Fig. 1(b). An overview image illustrates that the sample consists of BT-NWs on a large scale. The TEM image of typical BT-NWs is also shown in Fig 1(c). The diameter of this BT-NW is about 40 nm and length is about 1000 nm. The aspect ratio of this nanowire is about 25.

Characterization of Composites

We prepared two kinds of composites, which contain BT-NPs and BT-NWs, respectively.

Fig. 2 shows the XRD patterns of pure PVDF-HFP, PVDF-HFP/BT-NPs and PVDF-HFP/BT-NWs composites. The XRD pattern of pure PVDF-HFP can be indexed according to the α, β and γ PVDF crystalphases. The peak at 18.4 °corresponding to the PVDF α-phase, as well as the 20.8 ° peak and 26.6 ° broad peak that corresponds to the superposition of the β-phase and γ-phase diffraction, respectively.[34] For the composites, the characteristic diffraction peaks of $BaTiO_3$ appear at about 2θ =22 °, 31 °, 38 °, which are associated with typical structures of perovskite $BaTiO_3$ in crystal planes of (100), (110) and (111). After BT-NPs or BT-NWs were incorporated into the PVDF-HFP matrix, the XRD patterns of composites show those $BaTiO_3$ diffraction peaks, superimposed on top of PVDF-HFP background. The appearance of the characteristic diffraction peaks for $BaTiO_3$ clearly demonstrates that $BaTiO_3$ are fully filled in the polymer matrix.

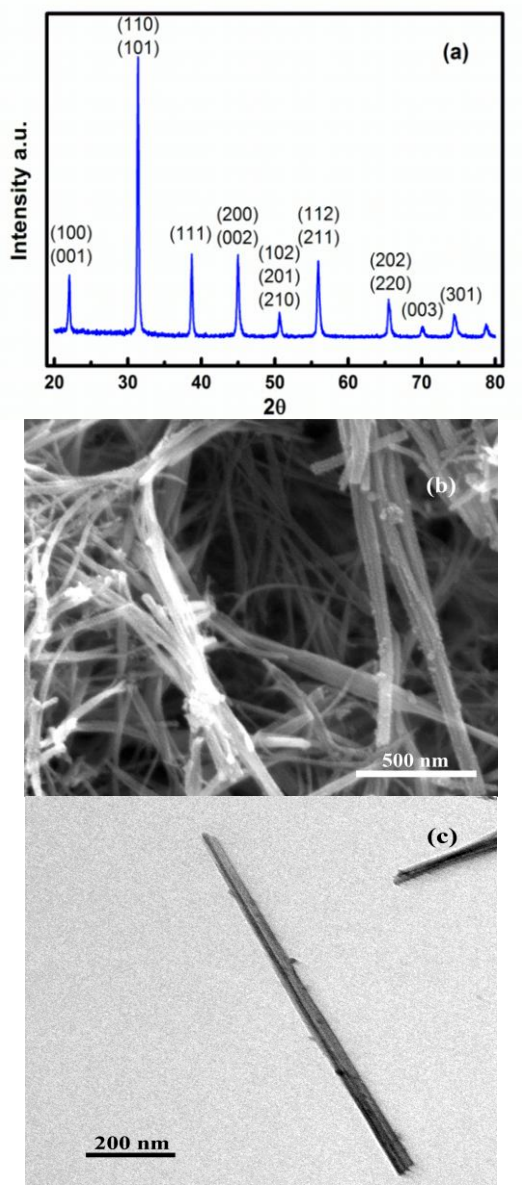

Figure 1. (a) XRD pattern, (b) SEM image and (c) TEM image of BT-NWs

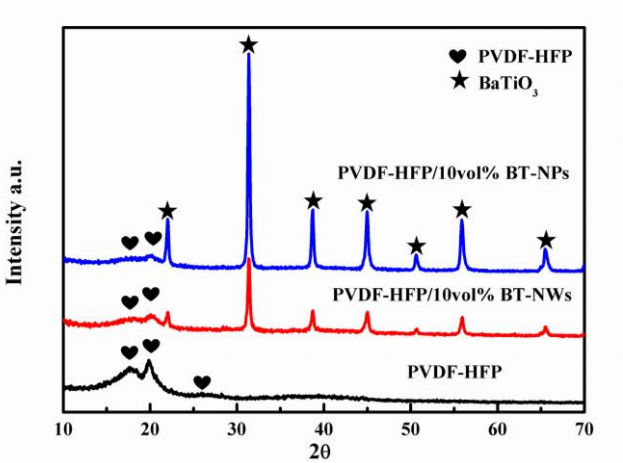

Figure 2. XRD patterns of PVDF-HFP, PVDF-HFP/BT-NPs and PVDF-HFP/BT-NWs composites.

FTIR experiments are performed and shown in Fig 3. All FTIR spectra of the five samples show the typical absorption peaks of α-phase, β-phase and γ-phase of PVDF-HFP at about 615 cm^{-1}, 511 cm^{-1} and 840 cm^{-1}, which indicate that the crystalline type of the composites are almost the same as the pure PVDF-HFP. The bending of C-C-C is also observed at 1070 cm^{-1}, while the peak of CH_2 appears at 1402 cm^{-1}.[35] Meanwhile, no peak of hydrogen bonds can be detected in pure PVDF-HFP. In the spectra of PVDF-HFP/BT-NPs and PVDF-HFP/BT-NWs composites, the absorption peaks range from 3250 cm^{-1} to 3500 cm^{-1} are attributed to the hydroxyl stretching vibration, which suggests that the strong hydrogen bonds are formed between the hydroxyl groups of BT fillers and fluoride atoms of PVDF-HFP.[36] In the case of PVDF-HFP/BT-NPs composites, the characteristic absorption peak due to the hydroxyl is observed at about 3511 cm^{-1}. For the composite filled by 2.5 vol% BT-NWs, the absorption peak of hydroxyl is detected at about 3390 cm^{-1}.The absorption peak of hydroxyl moves to 3369 cm^{-1} when the filler content increases to 10 vol%. The reduction of hydroxyl vibration energy suggests the formation of more stable hydrogen bonds. The similar result has been reported in other composite systems.[37]

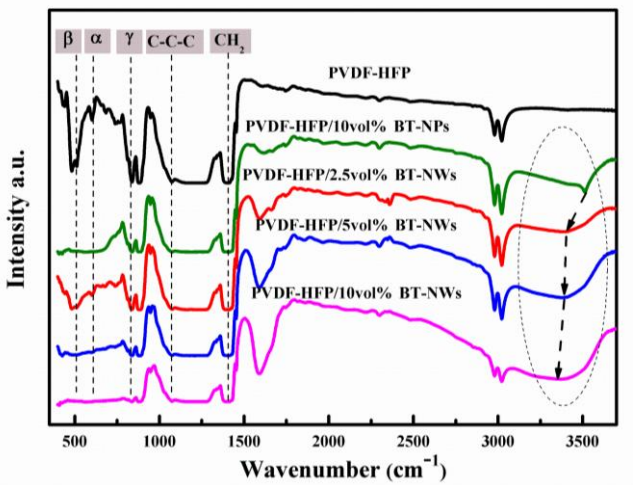

Figure 3. FTIR spectra of pure PVDF-HFP, PVDF-HFP/BT-NPs(10vol%), PVDF-HFP/ BT-NWs (2.5vol%, 5vol% and 10vol%) composites.

Fig. 4 displays cross section SEM images of pure PVDF-HFP, BT-NPs and composites. In order to protect the cross section morphology of composites, the fractured surfaces were prepared in liquid nitrogen. BT-NPs are clearly seen with rounded shapes and the sizes of particles are estimated on the order of 80-120 nm. Besides, in the Fig. 4 (d) and (f), BT-NPs and BT-NWs dispersing homogeneously into the PVDF-HFP matrices are found. However, there is a difference between above two kinds of composites. The interface between BT-NPs and the matrix is very clear, while that between BT-NWs and the matrix is so vague, which means that BT-NWs are coated by lots of PVDF-HFP. In this case, such a huge interfacial effect between PVDF-HFP and BT-NWs is stronger than that between PVDF-HFP and BT-NPs, and there should be powerful interface in the PVDF-HFP/BT-NWs composites.

Dielectric properties of composites

The dependency of the dielectric constant of composites with different contents on the frequency is shown in Fig. 5. With fillers (BT-NPs and BT-NWs) content increasing, the dielectric constant of the composites increases. The similar results are reported in previous papers.[13-16] With the frequency increasing, the dielectric constant of two composites both decrease, because the different types of polarizations will not keep up with the changing of the AC frequency and gradually vanish one by one.[38] Besides, dielectric constant of the two composites exhibits gradually increased frequency dependence as the fillers content increases, especially in frequency range of 0.01-10 Hz. Compared with the composites filled by BT-NPs, it is clearly demonstrated that the dielectric constant of the composite can be significantly improved by filling BT-NWs. For PVDF-HFP/10 vol% BT-NWs composites, the dielectric constant is about 9603, 391 and 49 at 0.01 Hz, 1 Hz and 100 Hz, respectively. However, the value of 10vol% PVDF-HFP/BT-NPs composite is only about 82, 25 and 16 respectively. It should be noted that the dielectric constant of the composite with 10 vol% BT-NWs can reach a dielectric constant as high as 49, which is three times higher than samples with 10 vol% BT-NPs (16) and five times larger than the polymer matrix (9.6) at 100 Hz.

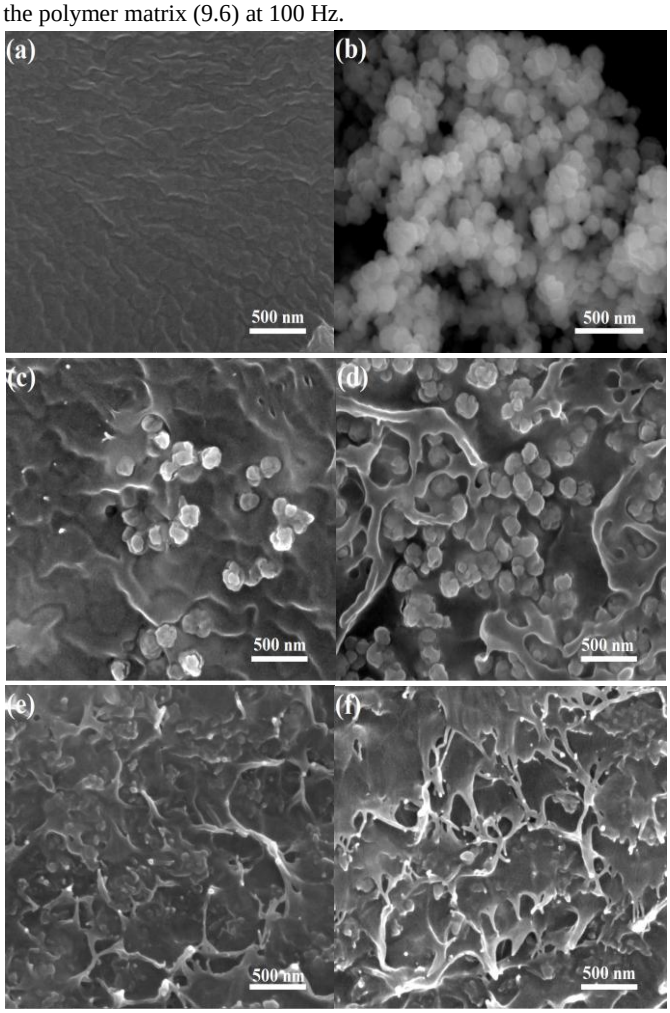

Figure 4. Cross section SEM images, (a) pure PVDF-HFP, (b) BT-NPs, (c) PVDF-HFP/2.5vol% BT-NPs, (d) PVDF-HFP/10vol% BT-NPs, (e) PVDF-HFP/2.5vol% BT-NWs, (f) PVDF-HFP/10vol% BT-NWs.

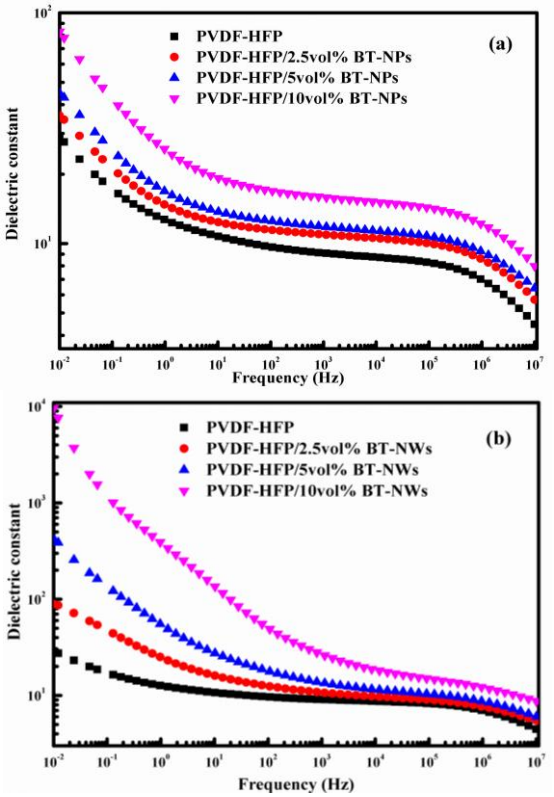

Figure 5. Dependence of dielectric constant of (a) PVDF-HFP/BT-NPs composites and (b) PVDF-HFP/BT-NWs composites with different filler contents on the frequency at room temperature.

Fig. 6 displays the dependence of alternating current (AC) conductivity of composites on the frequency in the 1×10^{-2} to 1×10^{7} Hz range. For both composites, the conductivity shows strong dependence on frequency owing to the insulating nature. The AC conductivity increase with the increasing frequency on the basis of an apparent power law: $\sigma(\omega)=\omega^{n}$ ($0.6 \le n \le 1$).[39] AC conductivity of both composites at lower frequency increases with the filler contents increasing. As the frequency $\geq 10^{4}$ Hz, the conductivity among PVDF-HFP/BT-NPs composites is almost same. The similar trend is found in the PVDF-HFP/BT-NWs composites. For the PVDF-HFP/BT-NWs composites, the value of frequency is 10^{6} Hz. For one kind of composite material system, when the fillers connect with each other and form long-range connectivity in the composites, we call this phenomenon as "percolation". The minimum volume fraction of fillers which can make the percolation take place is named as percolation threshold.[3] The effect of filler shape on the threshold value is significant. For example, the threshold value of spherical ceramic fillers is about 50-70 vol%, while only 0.5 wt% graphene oxide nanosheets can reach that value.[2, 5] The value of frequency where AC conductivity of composites filled by different contents becomes unequal can be used to reflect the threshold value. For PVDF-HFP/BT-NPs and PVDF-HFP/BT-NWs composite, the value of frequency is about 10^{4} Hz and 10^{6} Hz, respectively. So above results indicate that the threshold value for BT-NWs is smaller compared with BT-NPs, namely, it is easier for BT-NWs to reach the threshold value compared with the BT-NPs in the polymer matrix. AC conductivity of PVDF-HFP and PVDF-HFP/10vol% BT-NPs composite is 3.4×10^{-11} S/cm and 6.94×10^{-11} S/cm at 100 Hz, respectively. For the PVDF-HFP/10vol% BT-NWs composites, AC conductivity is 2.4×10^{-9} S/cm, which is far larger than that of PVDF-HFP/10vol% BT-NPs composites. It may be resulted from that the 10vol% content is close to the threshold value of BT-NWs in the PVDF-HFP matrix. Although the AC conductivity has an obviously increasing trend with the BT-NWs content increasing (0-10 vol%), AC conductivity of PVDF-HFP/BT-NWs composites still remains nearly frequency-dependent, which indicates that there are no an obvious insulator-to-conductor transition.

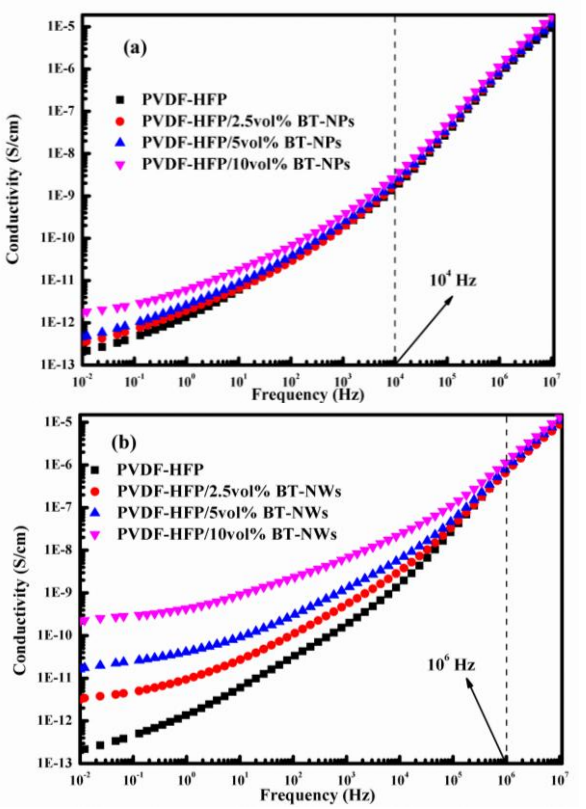

Figure 6. Dependence of electrical conductivity of (a) PVDF-HFP/BT-NPs and (b) PVDF-HFP/BT-NWs composites with different filler contents on the frequency at room temperature.

The dielectric loss ε'' describes the energy dissipation in a dielectric material through conduction (transport-related loss), slow polarization currents (dipolar loss), and other dissipative phenomena (interfacial polarization contribution).[40-42] For a composite, ε'' can be expressed as following equation

$$\varepsilon'' = \varepsilon_{dc}'' + \varepsilon_{MW}'' + \varepsilon_{D}'' \quad (1)$$

where ε_{dc}'' and ε_{MW}'' are related to conduction loss and interfacial polarization loss, respectively, and ε_{D}'' is the dipole loss factor.

The conduction loss factors ε_{dc}'' and interfacial polarization loss factor ε_{MW}'' are given by

$$\varepsilon_{dc}'' = \frac{\sigma_{dc}}{2\pi f} \quad (2)$$

where σ_{dc} and f represent the direct current conductivity and frequency, respectively. According to equation 2, log ε_{dc}'' versus log f represents a straight line.

$$\varepsilon_{MW}'' \propto \left(1 + \frac{K}{1+(2\pi f)^{2}\tau^{2}}\right) \quad (3)$$

where K is related to the dielectric constant of the films at the interface and τ is the relaxation time of the interfacial polarization. According to the equation 3, interfacial polarization versus frequency demonstrates a sigmoidal curve on a log-log plot.

Fig. 7 shows the dependence of log ε'' of PVDF-HFP/BT-NPs and PVDF-HFP/BT-NWs composites with different filler contents on the log (frequency) at room temperature. It appears that ε'' decreases with the frequency increasing at lower frequency then increases at higher frequency. It is generally believed that the high-frequency process is mainly associated with dipolar relaxation, whereas at lower frequency, the contributions of interfacial polarization and conductivity are significant. If only the conduction loss exists at lower frequency, log ε'' versus log f represents a straight line. In our paper, the plots of log ε'' versus log f do not show strict linear relationships at low frequency, indicating that the conduction loss is not dominant. The nonlinearity of conductivity especially is embodied in its rangeability and corresponding frequency range. The reason of nonlinearity is results from ε_{MW}'', because log ε_{MW}'' versus log f demonstrates a sigmoidal (nonlinear) curve. Thus, the more obvious nonlinearity in wider range of frequency observed in the PVDF-HFP/BT-NWs composites indicates that the interfacial polarization in PVDF-HFP/BT-NWs composites is stronger than that in PVDF-HFP/BT-NPs composites.

In order to show more information about the interfacial mechanism of the composites, the dielectric modulus formalism is given in Fig. 8. The advantages of the electric modulus formalism to interpret bulk relaxation properties over others are their independence of electrode nature and contact, space charge injection, and absorbed impurity conduction, which appear to obscure relaxation in the dielectric spectrum formalism. Electric modulus, M*, is defined by the following equation [43]

$$M^* = \frac{1}{\varepsilon^*} = \frac{1}{\varepsilon' - j\varepsilon''} = \frac{\varepsilon'}{\varepsilon'^2 + \varepsilon''^2} + j\frac{\varepsilon''}{\varepsilon'^2 + \varepsilon''^2} = M' + jM'' \quad (4)$$

The imaginary part (M'') of the electric modulus takes the form of loss curves, allowing us to interpret the relaxation phenomena. Up to now, the electric modulus formalism has been utilized to investigate interfacial polarization in several composites.[44, 45] Because the relaxation time of interfacial polarization is a little long, the peak of M'' at lower frequency represents the interfacial polarization. The right movement of this peak in the frequency spectrum can illustrate the enhancement of interfacial polarization. It can be observed that a relaxation peaks associated with interfacial polarization of the two types of composites both appear at lower frequency. With the BT content increasing, the relaxation peak moves to the higher frequency, which indicates that the incorporation of BT raises the interfacial polarization in two types of composites. Apparently, the shift of PVDF-HFP/BT-NWs composites is ever more significant, namely, the interfacial polarization in PVDF-HFP/BT-NWs composites is stronger than that in PVDF-HFP/BT-NPs composites. The similar result has been reported in numerous composite systems.[44, 46] The M'' curve of the pure PVDF-HFP also shows an interfacial relaxation peak, which is due to the charge accumulation on the boundary between the lamellar crystal and interlamellar amorphous region.[46]

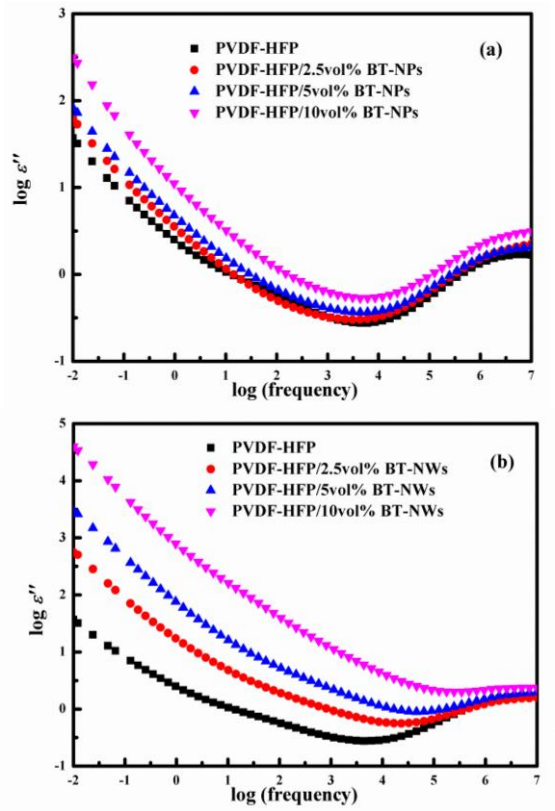

Figure 7. Dependence of dielectric loss of (a) PVDF-HFP/BT-NPs and (b) PVDF-HFP/BT-NWs composites with different filler contents on the frequency at room temperature.

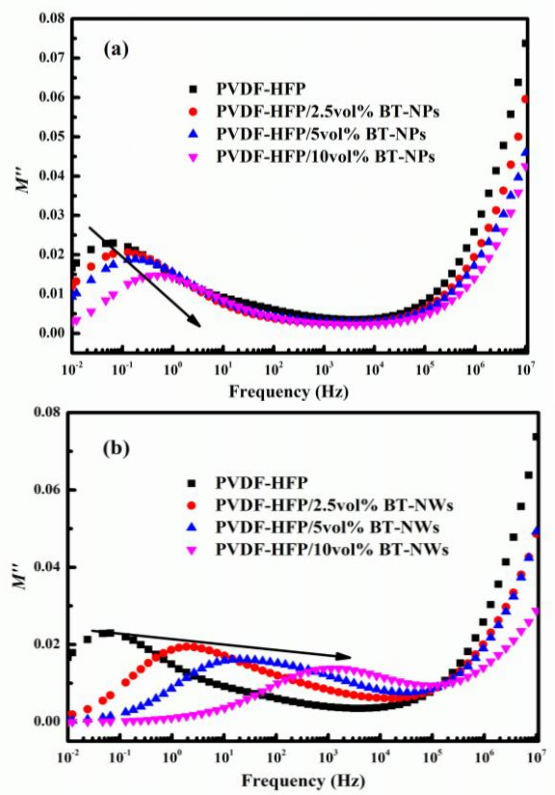

Figure 8. Dependence of the imaginary part of electric modulus of (a) PVDF-HFP/ BT-NPs and (b) PVDF-HFP/BT-NWs composites with different filler contents on the frequency at room temperature.

Breakdown strength and tensile strength of composites

An excellent property of a dielectric material is not only its ability to increase capacitance, but also, and equally important, its insulating behavior and mechanical performance. The breakdown strengths and tensile strengths of the PVDF-HFP/BT-NPs and PVDF-HFP/BT-NWs composites were carried out, and the results are provided in Fig. 9. With the filler content increasing, the breakdown strengths of two kinds of composites both decrease; however, the breakdown strength of PVDF-HFP/BT-NWs composites is lower than that of PVDF-HFP/BT-NPs composites at same filler content, which is agreement with previous conductivity data. Apparently, it is easier to form breakdown tunnel in the composites filled by one-dimension filler than that filled by zero-dimension filler. For the PVDF-HFP/10vol% BT-NWs composite, the breakdown strength, however, is still higher than 90 kV/mm, which proves its excellent insulating behavior.

As the content of two fillers increasing from 0vol% to 10vol% in respective polymer matrix, the changing trends for tensile strength are in an different way: the tensile strength of PVDF-HFP/BT-NWs composites rises from 31.17 to 41.77 MPa and the tensile strength of PVDF-HFP/BT-NPs composites approximately keeps unchanged (31.17~33.33 MPa). Theoretically, one dimensional material in the composites can share more external stress, which should have loaded on the polymer matrix. The similar results are reported in previous papers, which cover the enhanced effect of the CNT on the tensile strength of polymer/CNT composites.[47, 48] One dimensional materials used in the fabrication of other constructional composites are usually researched and the enhanced mechanisms are also the focus of many papers.[49, 50]

These results are important for practical application because that the PVDF-HFP/BT-NWs composites have higher dielectric properties and electrical breakdown strength without lowing mechanical property.

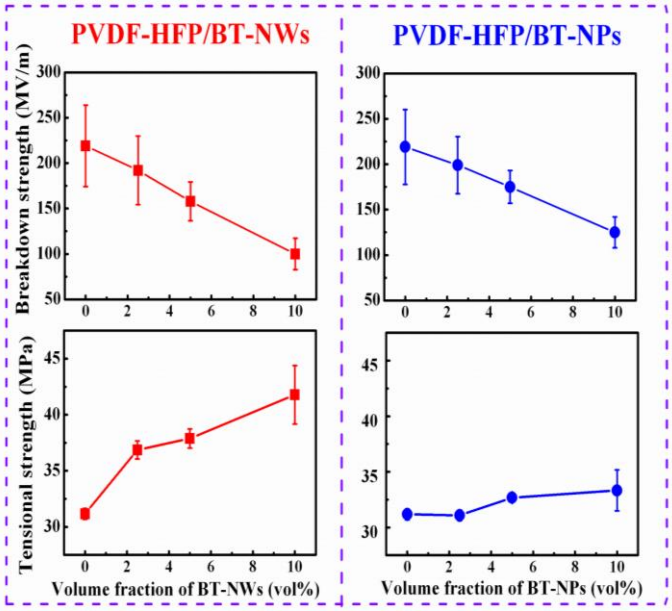

Figure 9. Electrical breakdown strength and tensile strength of two types of composites

Discussions

Owing to the enhancement of dielectric constant induced by the BT-NWs are closely related with frequency, especially at lower frequency region, the variation of dielectric constant of the composites with BT-NWs and BT-NPs filler at different frequency are shown in Fig. 10. It can be seen that, at 10^{-2} Hz, the dielectric constant of PVDF-HFP/10 vol% BT-NWs composite is 9603, which is 120 times larger than that (82) of the composites filled by 10 vol% BT-NPs. At 1 Hz, dielectric constant is 391, which is 15.2 times larger than that (25) of composites filled by BT-NPs. Meanwhile, at 10^{2} Hz, dielectric constant is 49, which is 3 times larger than that (16.8) of the composites filled by BT-NPs.

It is clear that the PVDF-HFP/BT-NWs composites show obviously enhanced dielectric constant compared with the PVDF-HFP/BT-NPs composites at lower frequency (≤10 Hz). However, with the frequency increasing (≥10 Hz), the dielectric constant ratio of PVDF-HFP/BT-NWs to PVDF-HFP/BT-NPs composites diminishes gradually. It is possible resulted from that the stronger interfacial polarization exists in the PVDF-HFP/BT-NWs composites, and the influence from interfacial polarization on the dielectric constant decreases with the frequency increasing. [51]

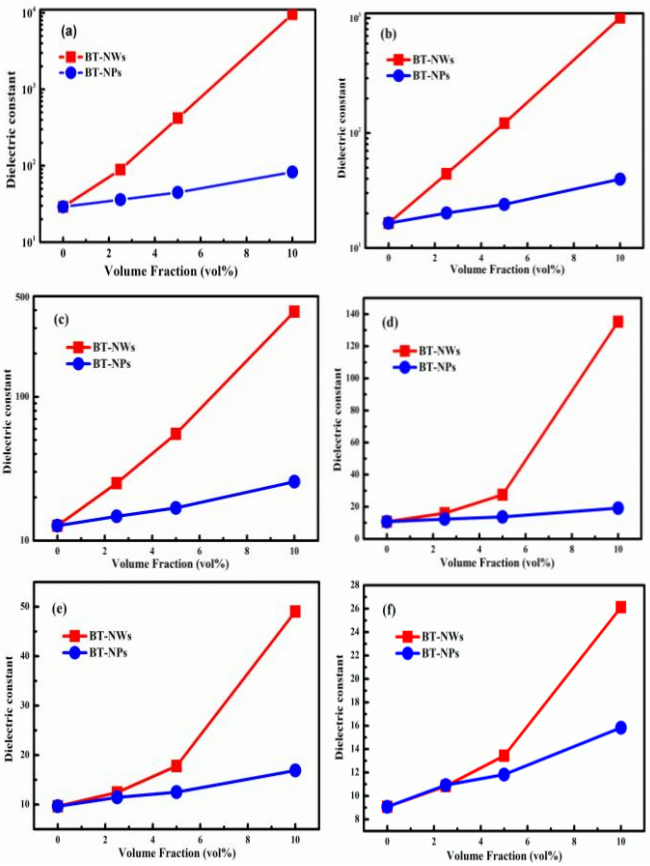

Figure 10. Dielectric constant of PVDF-HFP/BT-NWs and PVDF-HFP/BT-NPs composites at (a) 0.01 Hz, (b) 0.1 Hz, (c) 1 Hz, (d) 10 Hz, (e)100 Hz and (f)1000 Hz.

To further demonstrate that interfacial effect existing in the PVDF-HFP/BT-NWs composites is stronger than that of PVDF-HFP/BT-NPs composites, the activation energy (E_a) of the composites was calculated. According to the Arrhenius law the conductivity (σ) is strongly dependent on temperature (T), and the equation can be written as:

$$\sigma(T) = \sigma_0 \exp(-\frac{E_a}{kT}) \quad (5)$$

where σ_0 is a pre-exponential term and represents the high temperature limit of conductivity, while k and T are the Boltzmann constant and the absolute temperature, respectively. The E_a, which can be obtained from the plots of lnσ versus 1000/T, reflects the intensity of interfacial polarization.[52, 53]

Fig. 11 shows the dependence of lnσ on 1000/T at 100 Hz for the pure PVDF-HFP, PVDF-HFP/10vol% BT-NWs and PVDF-HFP/10vol% BT-NPs composites. It is clear that the curves of pure PVDF-HFP and PVDF-HFP/BT-NPs composite over the whole range could be fitted to straight line. The calculated E_a of the pure PVDF-HFP and PVDF-HFP/BT-NPs composite is 0.52 eV and 0.083 eV, respectively. The E_a of PVDF-HFP is reduced due to the incorporation of BT-NPs. Meanwhile, the E_a of PVDF-HFP and PVDF-HFP/BT-NPs composite is still positive. However, the E_a of PVDF-HFP/BT-NWs composite is different from other two. As shown in the Fig. 11, negative E_a (E_a=-0.263 eV) is found in the wide range of lower temperature in the PVDF-HFP/BT-NWs composite. The positive activation energy implies that the movement of electrons is restricted and the free charges available at the interface move difficultly in the PVDF-HFP and PVDF-HFP/BT-NPs composite when an electric field is applied. However, the negative activation energy indicates that a large number of electrons are possible present at the interface of the PVDF-HFP/BT-NWs composites, then results in strong interfacial polarization. The experimental results confirm what we expected. The improvement of dielectric constant in PVDF-HFP/BT-NWs composites is attributed to the enhancement of interfacial polarization.

In view of the previous data on dielectric loss and conductivity, we find that the dielectric properties of PVDF-HFP/BT-NWs composites are similar to that of PVDF/conductive fillers: higher dielectric loss, conductivity, and negative E_a. It is possible resulted from following reason: the BT-NWs are synthesized via hydrothermal method. There should be a few oxygen vacancies introduced in the lattice of BT-NWs during the chemical synthetic process. Due to the existence of oxygen vacancies, a few shallow donors are formed around the oxygen vacancies. Under electric field or thermal excitation, it is easy for the shallow donors to generate charge carriers. The characters of carriers generated by shallow donors are similar to that in the conductive fillers. The only difference is that the concentration of carriers generated by shallow donors is so low compared with that in conductive fillers. Thus, higher dielectric loss, conductivity and negative E_a are observed in PVDF-HFP/BT-NWs composites.

When the temperature is lower, the carriers can be easily excited and participate in conduction and interfacial polarization, thus E_a in the PVDF-HFP/BT-NWs composite is negative. With the temperature increasing, no more carriers can be excited by shallows donors and take part in the conduction, so E_a becomes positive again in the PVDF-HFP/BT-NWs composite.

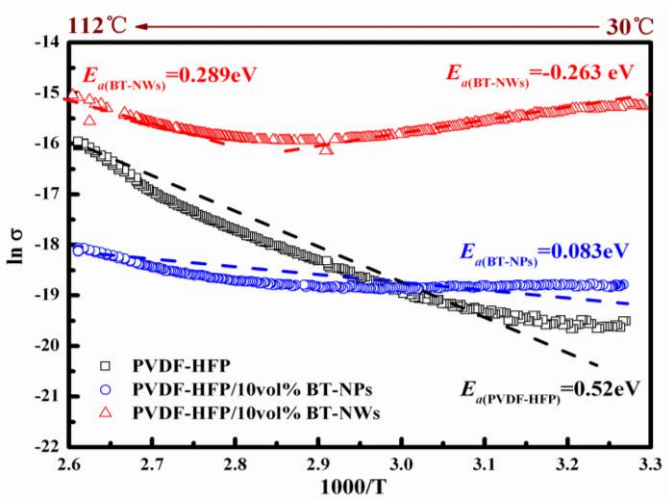

Figure 11. Dependence of lnσ on 1000/T for the PVDF-HFP, PVDF-HFP/BT-NPs and PVDF-HFP/BT-NWs composites at 100 Hz

As discussed above, the interfacial polarization will diminish gradually with frequency increasing. Meanwhile, the enhancement of dielectric constant resulting from interfacial polarization will also decrease then vanish. However, the dielectric constant of PVDF-HFP/BT-NWs composites is still larger than that filled by BT-NPs at higher frequency. The largest distinction between BT-NPs and BT-NWs is the shape and aspect ratio. The effect of distinction above on the dielectric constant can be reflected by using different effective medium models. The enhanced dielectric constant induced by various shape of filler have be researched in many papers, and effective medium models for several filler shapes (sphere-shaped, ellipsoid-shaped or needle-shaped) have been developed.[23, 54-56]

The polarization of the composite is a function of the filler geometry and orientation with respect to the applied field. The depolarization factors (N_x, N_y, N_z) describe the extent to which the inclusion polarization is reduced, according to its shape and orientation along each semiaxis of the ellipsoid.[57] The depolarization factors are calculated from integrals by following equation:

$$N_x = \frac{a_x a_y a_z}{2} \int_0^\infty \frac{1}{(s+a_x^2)\sqrt{(s+a_x^2)(s+a_y^2)(s+a_z^2)}} ds \quad (6)$$

where a_x, a_y, and a_z are the semiaxes of the filler. For the case of spherical filler, all three depolarization factors are equal (1/3, 1/3, 1/3), and the dielectric constant are estimated using the Maxwell-Garnett (MG) effective medium theory (equation 7), and for the case of randomly aligned ellipsoidal or wire-like inclusions, the depolarization factors are (0, 1/2, 1/2), and the dielectric constant are estimated using the Polder-Van Santen (PVS) formalism (equation 8),

$$\varepsilon_{eff} = \varepsilon_b \left[\frac{\varepsilon_a + 2\varepsilon_b + 2v_a(\varepsilon_a - \varepsilon_b)}{\varepsilon_a + 2\varepsilon_b - v_a(\varepsilon_a - \varepsilon_b)} \right] \quad (7)$$

$$\varepsilon_{eff} = \varepsilon_b + \frac{v_a}{3}(\varepsilon_a - \varepsilon_b) \sum_{j=x,y,z} \frac{\varepsilon_{eff}}{\varepsilon_{eff} + N_j(\varepsilon_a - \varepsilon_{eff})} \quad (8)$$

where ε_a is the dielectric constant of the $BaTiO_3$ fillers, ε_b the dielectric constant of PVDF-HFP, v_a the volume fraction of $BaTiO_3$ fillers, and the N_j represents the depolarization factors.

Fig. 12 shows that a substantial enhancement in ε_{eff} is predicted for ellipsoidal inclusions, compared to spherical inclusions. The enhancement is clearly greatest for ellipsoidal inclusions, because of their larger dipole moments (versus spherical shapes).[56-58]

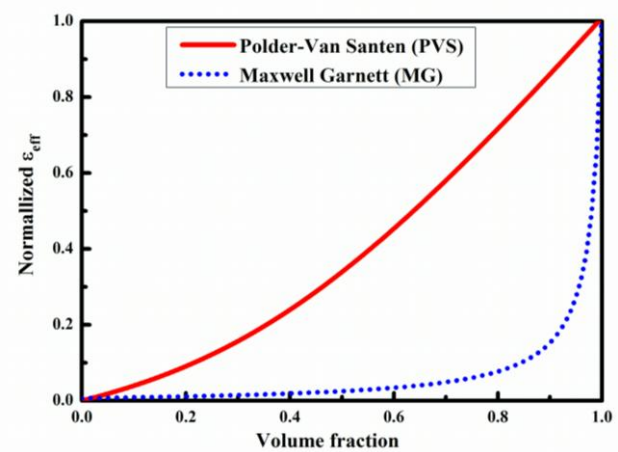

Figure 12. Normalized calculated effective permittivity $((\varepsilon_{eff} - \varepsilon_b)/(\varepsilon_a - \varepsilon_b))$ for composite dielectrics with spherical inclusions (denoted by the dashed line) and ellipsoidal inclusions (denoted by the solid line).

The comparison of PVDF-HFP/BT-NWs and PVDF-HFP/BT-NPs composites is plotted in Fig. 13. It can be seen that the uptrends of dielectric constant of two types of composites are consistent with the predicted trends in Fig. 12. Hence, we suppose that the various aspect ratio results in the difference of depolarization factors. The depolarization factors of fillers, then, will influent the polarization of the composite. Finally, the variation of dielectric properties should be due to the different aspect ratio between two types of fillers.

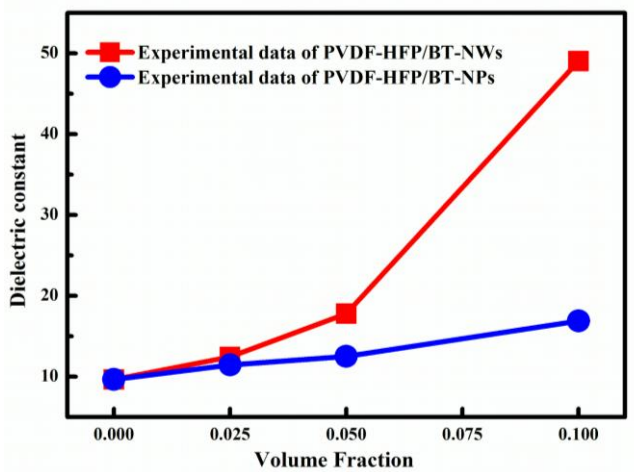

Figure 13. Comparison of experimental data for composites containing BT-NPs and BT-NWs at 100 Hz.

Conclusions

PVDF-HFP composites filled by two types of fillers ($BaTiO_3$ nanowires and nanoparticles) were fabricated by in-situ dispersive polymerization. BT-NWs with high aspect ratio were synthesized by one-step hydrothermal method. The results of XRD, FTIR, SEM and TEM provide the evidences that two types of fillers are successfully incorporated into PVDF-HFP matrix. With $BaTiO_3$ content increasing, enhancements of the dielectric constant are found in two types of composites. The dielectric constant of PVDF-HFP/$BaTiO_3$-NWs composites is obviously larger than that of PVDF-HFP/BT-NPs composites and pure PVDF-HFP. The interfacial polarization in PVDF-HFP/BT-NWs is stronger than that in PVDF-HFP/BT-NPs composites, which is proved via calculating the activation energy (E_a). The stronger interfacial polarization in PVDF-HFP/BT-NWs composites is the reason that dielectric constant of PVDF-HFP/BT-NWs composites dominates that of PVDF-HFP/BT-NPs composites at lower frequency. Besides, the increasing trends of dielectric constant in two types of composites agree well with the MG and PVS models, respectively. We believe that the high aspect ratio of BT-NWs, which is the another crucial factor, results in the larger dielectric constant in PVDF-HFP/BT-NWs composites.

In a word, we fabricated a kind of high-ε polymer based composite with low inorganic content (≤ 10 vol%), which has excellent insulating behavior without lowing mechanical property. The method of preparing above materials is to incorporate high aspect ratio ceramic nanowires into polymer, which is also a guideline in further electronics industry, for applications such as printed circuit boards (PCBs).

Acknowledgements

This work was financially supported by the National Nature Science Foundation of China (Grant No. 11272102). The authors gratefully acknowledge the help from Prof. Jinghua Yin and Dr. Lei Yao at dielectric properties measurement.

Notes and references

1 B. J. Chu, X. Zhou, K. L. Ren, B. Neese, M. R. Lin, Q. Wang, F. Bauer, Q. M. Zhang, *Science*, 2006, **313**, 334-336.

2 Z. M. Dang, T. Zhou, S. H. Yao, J. K. Yuan, J. W. Zha, H. T. Song, J. Y. Li, Q. Chen, W. T. Yang, J. Bai, *Adv. Mater.*, 2009, **21**, 2077-2082.

3 G. S. Wang, *ACS Appl. Mater. Interfaces*, 2010, **2**, 1290– 1293.

4 J. W. Zha, W. K. Li, R. J. Liao, J. B. Bai, Z. M. Dang, *J. Mater. Chem. A*, 2013, **1**, 843-851.

5 F. Liu, R. M. Huo, X. Y. Huang, Q. Q. Lei and P. K. Jiang, *IEEE T. Dielect. El. In.*, 2014, **21**, 1446-1454.

6 J. J. Li, S. I. Seok, B. J. Chu, F. Dogan, Q. M. Zhang, Q. Wang, *Adv. Mater.*, 2009, **21**, 217-221.

7 Q. M. Zhang, H. F. Li, M. Poh, F. Xia, Z. Y. Cheng, H. S. Xu, C. Huang, *Nature*, 2002, **419**, 284-287.

8 K. Yang, X. Y. Huang, M. Zhu, L. Y. Xie, T. Tanaka and P. K. Jiang, *ACS Appl. Mater. Interfaces*, 2013, **6**, 1812-1822.

9 X. Y. Huang and P. K. Jiang, *Adv. Mater.*, 2014, DOI: 10.1002/adma.201401310.

10 K. Yang, X. Y. Huang, Y. H. Huang, L. Y. Xie and P. K. Jiang, *Chem. Mater.*, 2013, **25**, 2327−2338.

11 P. H. Hu, Y. Shen, Y. H. Guan, X. H. Zhang, Y. H. Lin, Q. M. Zhang and C. W. Nan, *Adv. Funct. Mater.*, 2014, **24**, 3172–3178.

12 X. Zhang, W. W. Chen, J. J. Wang, Y. Shen, G. Lin, Y. H. Lin and C. W. Nan, *Nanoscale*, 2014, **6**, 6701-6709.

13 M. Arbatti, X. B. Shan, Z. Y. Cheng, *Adv. Mater.*, 2007, **19**, 1369-1372.

14 H. M. Jung, J. H. Kang, S. Y. Yang, J. C. Won, Y. S. Kim, *Chem. Mater.*, 2010, **22**, 450-456.

15 E. A. Stefanescu, X. L. Tan, Z. Q. Lin, N. Bowler, M. R. Kessler, *Polymer*, 2011, **52**, 2016-2024.

16 S. J. Chang, W. S. Liao, C. J. Ciou, J. T. Lee, C. C. Li, *J. Colloid Interf. Sci*., 2009, **329**, 300-305.
17 V. K. Thakur, E. J. Tan, M. F. Lin, P. S. Lee, *J. Mater. Chem.*, 2011, **21**, 3751-3759.
18 Y. Deng, Y. J. Zhang, Y. Xiang, G. S. Wang, H. B. Xu, *J. Mater. Chem.*, 2009, **19**, 2058-2061.
19 K. Arlt, M. Wegener, *IEEE T. Dielect. El. In.*, 2010, **17**, 1178-1184.
20 B. C. Luo, X. H. Wang, Y. P. Wang, L. T. Li, *J. Mater. Chem. A*, 2014, **2**, 510-519.
21 H. X. Tang, M. H. Malakooti, H. A. Sodano, *Appl. Phys. Lett.*, 2013, **103**, 222901.
22 S. H. Liu, J. W. Zhai, J. W. Wang, S. X. Xue, W. Q. Zhang, *Acs Appl. Mater. Inter*., 2014, **6**, 1533-1540.
23 M. C. Araujo, C. M. Costa, S. Lanceros-Mendez, *J. Non-Cryst. Solids*, 2014, **387**, 6-15.
24 A. B. da Silva, M. Arjmand, U. Sundararaj, R. E. S. Bretas, *Polymer*, 2014, **55**, 226-234.
25 P. Potschke, S. M. Dudkin, I. Alig, *Polymer*, 2003, **44**, 5023-5030.
26 R. R. Kohlmeyer, A. Javadi, B. Pradhan, S. Pilla, K. Setyowati, J. Chen, S. Q. Gong, *J. Phys. Chem. C*, 2009, **113**, 17626-17629.
27 H. X. Tang, Z. Zhou, H. A. Sodano, *ACS Appl. Mater. Interfaces*, 2014, **6**, 5450-5455.
28 H. X. Tang, Y. R. Lin, H. A. Sodano, *Adv. Energy Mater.*, 2012, **2**, 469–476.
29 H. X. Tang, Y. R. Lin, H. A. Sodano, *Adv. Energy Mater.*, 2013, **3**, 451–456.
30 H. X. Tang, H. A. Sodano, *Nano Lett*. 2013, **13**, 1373-1379.
31 N. Guo, S. A. DiBenedetto, P. Tewari, M. T. Lanagan, M. A. Ratner, T. J. Marks, *Chem. Mater*., 2010, **22**, 1567-1578.
32 Y. Song, Y. Shen, H. Y. Liu, Y. H. Lin, M. Li, C. W. Nan, *J. Mater. Chem.*, 2012, **22**, 16491-16498.
33 J. Yang, J. Zhang, C. Y. Liang, M. Wang, P. F. Zhao, M. M. Liu, J. W. Liu and R. C. Che, *ACS Appl. Mater. Interfaces*, 2013, **5**, 7146-7151.
34 W. Z. Ma, J. Zhang, S. J. Chen, X. L. Wang, *Appl. Surf. Sci.*, 2008, **254**, 5635-5642.
35 S. Lanceros-Mendez, J. F. Mano, A. M. Costa, V. H. Schmidt, *J. Macromol. Sci. Phys.*, 2001, **B40**, 517-527.
36 A. T. Chien, X. Xu, J. H. Kim, J. Sachleben, J. S. Speck, F. F. Lange, *J. Mater. Res.*, 1999, **14**, 3330-3339.
37 D. R. Wang, Y. R. Bao, J. W. Zha, J. Zhao, Z. M. Dang, G. H. Hu, *Acs Appl. Mater. Inter*., 2012, **4**, 6273-6279.
38 K. C. Kao, *Dielectric Phenomena in Solids*. Academic Press Inc. 2004.
39 J. C. Dyre, T. B. Schroder. *Rev. Mod. Phys.*, 2000, **72**, 873–92.
40 L. Y. Xie, X. Y. Huang, C. Wu, P. K. Jiang, *J. Mater. Chem.*, 2011, **21**, 5897-5906.
41 B. G. Soares, M. E. Leyva, G. M. O. Barra, D. Khastgir, *Eur. Polym. J.*, 2006, **42**, 676-686.
42 A. Fattoum, F. Gmati, N. Bohli, M. Arous, A. B. Mohamed, *J. Phys. D Appl. Phys*., 2008, **41**, 095407.
43 S. Havriliak, Negami, S., *Polymer*, 1967, **8**, 50.
44 M. Laurati, P. Sotta, D. R. Long, L. A. Fillot, A. Arbe, A. Alegria, J. P. Embs, T. Unruh, G. J. Schneider, J. Colmenero, *Macromolecules*, 2012, **45**, 1676-1687.
45 G. M. Tsangaris, G. C. Psarras, N. Kouloumbi, *J. Mater. Sci.*, 1998, **33**, 2027-2037.
46 X. Y. Huang, C. Y. Zhi, P. K. Jiang, D. Golberg, Y. Bando, T. Tanaka, *Nanotechnology*, 2012, **23**, 455705
47 K. Sugano, M. Kurata, H. Kawada, *Carbon*, 2014, **78**, 356-365.
48 M. Nie, D. M. Kalyon, F. T. Fisher, *ACS Appl. Mater. Interfaces*, 2014, **6**, 14886-14893.
49 W. D. Fei, Y. B. Li, *Mat. Sci. Eng. A*, 2004, **379**, 27-32.
50 H. Q. Gao, L. D. Wang, W. D. Fei, *Mat. Sci. Eng. A*, 2008, **479**, 261-268.
51 Y. Feng, J. H. Yin, M. H. Chen, M. X. Song, B. Su, Q. Q. Lei, *Mater. Lett.*, 2013, **96**, 113-116.
52 W. H. Yang, S. H. Yu, R. Sun, R. X. Du, *Acta Mater*., 2011, **59**, 5593-5602.
53 Q. G. Chi, J. Sun, C. H. Zhang, G. Liu, J. Q. Lin, Y. N. Wang, X. Wang, Q. Q. Lei, *J. Mater. Chem. C*, 2014, **2**, 172-177.
54 Z. M. Dang, J. K. Yuan, J. W. Zha, T. Zhou, S. T. Li, G. H. Hu, *Prog. Mater. Sci.*, 2012, **57**, 660-723.
55 N. G. Green, T. B. Jones, *J. Phys. D Appl. Phys.*, 2007, **40**, 78-85.
56 L. Jylha, A. Sihvola, *J. Phys. D Appl. Phys.*, 2007, **40**, 4966-4973.
57 S. B. Jones, S. P. Friedman, *Water Resour. Res.*, 2000, **36**, 2821-2833.
58 J. P. Adohi, C. V. Bouanga, K. Fatyeyeva, M. Tabellout, *J. Phys. D Appl. Phys*., 2009, **42**, 015302.

Table of concents entry

A high-ε polymer based composite with lower inorganic content (≤ 10 vol%) was fabricated by using the $BaTiO_3$ nanowires as fillers.